The Influence of Current Density and Magnetic Field Topography in Optimizing the Performance, Divergence, and Plasma Oscillations of High Specific Impulse Hall Thrusters

Richard R. Hofer*
QSS Group, Inc.
Cleveland, OH 44135 USA
richard.hofer@grc.nasa.gov

Robert S. Jankovsky†
NASA Glenn Research Center
Cleveland, OH 44135 USA

ABSTRACT

Recent studies of xenon Hall thrusters have shown peak efficiencies at specific impulses of less than 3000 s. This was a consequence of modern Hall thruster magnetic field topographies, which have been optimized for 300 V discharges. On-going research at the NASA Glenn Research Center is investigating this behavior and methods to enhance thruster performance. To conduct these studies, a laboratory model Hall thruster that uses a pair of trim coils to tailor the magnetic field topography for high specific impulse operation has been developed. The thruster—the NASA-173Mv2—was tested to determine how current density and magnetic field topography affect performance, divergence, and plasma oscillations at voltages up to 1000 V. Test results showed there was a minimum current density and optimum magnetic field topography at which efficiency monotonically increased with voltage. At 1000 V, 10 mg/s the total specific impulse was 3390 s and the total efficiency was 60.8%. Plume divergence decreased at 400–1000 V, but increased at 300–400 V as the result of plasma oscillations. The dominant oscillation frequency steadily increased with voltage, from 14.5 kHz at 300 V, to 22 kHz at 1000 V. An additional oscillatory mode in the 80–90 kHz frequency range began to appear above 500 V. The use of trim coils to modify the magnetic field improved performance while decreasing plume divergence and the frequency and magnitude of plasma oscillations.

I. INTRODUCTION

Expanding the operating envelope of Hall Effect Thruster (HET) technology has been the subject of several investigations conducted at the NASA Glenn Research Center (GRC).[1] As part of this program, research on the physical limits of HETs—in terms of power and specific impulse (Isp)—is being conducted. Separate studies at GRC have demonstrated power levels of 72 kW and Isp of 4100 s with xenon HETs.[2,3] This paper discusses continuing efforts at GRC to develop efficient, high-Isp thrusters.

While state-of-the-art HETs are designed for 300 V, there are no fundamental limitations of operating at higher voltages and thereby higher Isp. The challenge is maintaining efficient operation while increasing Isp. This became evident during high-Isp testing of three laboratory model HETs: the Boeing/TsNIIMASH D-80, the ARC/Fakel SPT-1 and the Busek BHT-1000.[3-5] These tests confirmed the functional relationship between anode Isp and discharge voltage as shown in Figure 1. However, maximum anode efficiency was limited to less than 3000 s Isp, as shown in Figure 2. The voltage at which efficiency peaked was found between 500–800 V and depended both on the mass flow rate and the thruster.

The subject of current investigations is to eliminate the efficiency peak and understand the physical mechanisms of the phenomenon. To conduct these investigations the NASA-173Mv1 and NASA-173Mv2 laboratory model HETs have been designed and fabricated by GRC.[6-7] The hypothesis when building both thrusters was that the magnetic field topography required for efficient, high-voltage operation would differ from that employed at 300 V. The NASA-173M thrusters therefore employ magnetic circuits that allow for significant variations of the field topography.

A recent performance characterization of the 173Mv1 has confirmed the hypothesis.[7] An internal trim coil (ITC) was used to alter the field topography during a performance mapping from 300–1000 V. Figure 3 shows the 173Mv1 efficiency at 5 mg/s with and without the ITC. The results demonstrated that the efficiency peak observed without the ITC could be mitigated when the magnetic field topography was tailored for high-voltage. The goal with the next thruster, the 173Mv2, was to completely eliminate the

* Research Scientist
† Chief, On-Board Propulsion Branch

.

efficiency peak. The tests reported in this paper were conducted to evaluate whether this goal was achieved by exploring the operating envelope of the 173Mv2. Performance of the 173Mv2 was mapped while varying the discharge voltage from 300–1000 V at 5–10 mg/s and 300–600 V at 15 mg/s. Ion current density and plasma oscillation data were also collected at 10 mg/s.

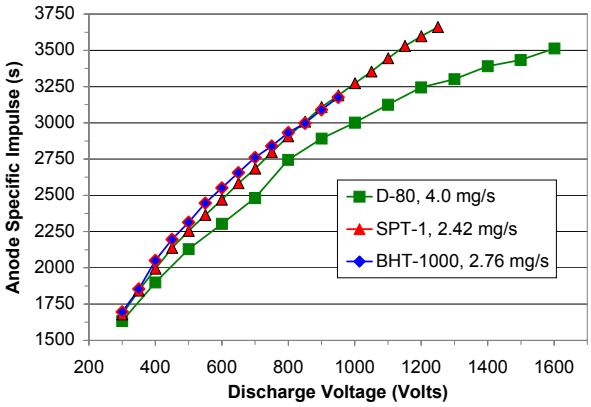

Figure 1 – Representative data of the anode specific impulse versus discharge voltage for the D-80, SPT-1, and BHT-1000.[3-5]

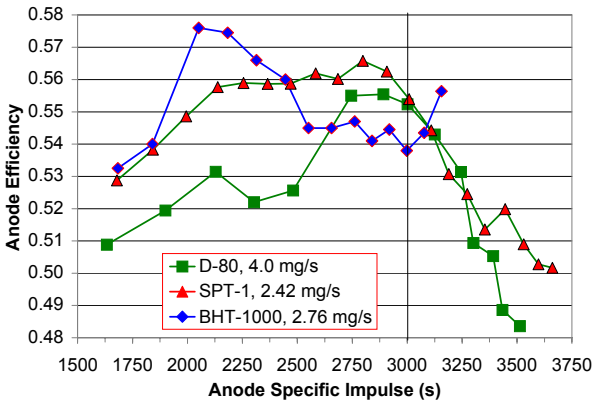

Figure 2 – Representative data of the anode efficiency versus anode specific impulse for the D-80, SPT-1, and BHT-1000.[3-5]

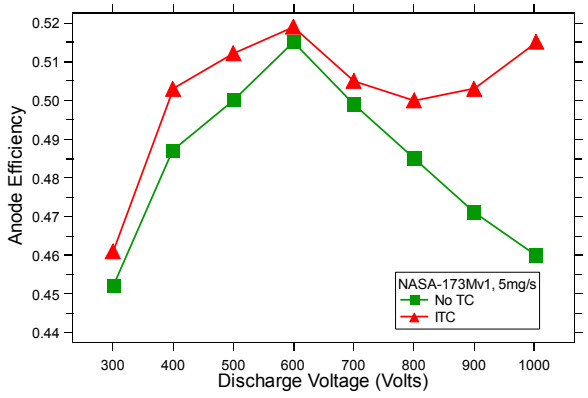

Figure 3 – Anode efficiency versus voltage at 5 mg/s in the NASA-173Mv1 with no trim coil (No TC) and with the internal trim coil (ITC).[7]

II. EXPERIMENTAL APPARATUS

A. NASA-173Mv2 Hall effect thruster

Figure 4 is a photograph of the laboratory model NASA-173Mv2. The 173Mv2 is an evolved version of the 173Mv1, which has been described previously.[6-7] Both thrusters are nominally 5 kW HETs and are classified as magnetic layer or stationary plasma thrusters (SPT). The thrusters share the same gas injection schemes and discharge chamber geometry. The primary differences between the thrusters are improvements that were made in the 173Mv2 magnetic circuit, thermal design, assembly scheme and mass.

Figure 4 – The NASA-173Mv2 Hall effect thruster.

The magnetic field topography in the discharge chamber of both thrusters employ what is commonly referred to as a plasma lens.[6-7] In a plasma lens, the field line curvature preferentially focuses ions on the channel centerline away from the walls, which improves performance and thermal margin, decreases plume divergence and increases lifetime. This focusing effect is possible because magnetic field lines form equipotentials of the accelerating voltage (at least to a first order approximation.)[8] The plasma lens in the 173Mv2 is qualitatively similar to that of the 173Mv1. However, improvements to the lens curvature and symmetry were incorporated in the 173Mv2. The changes were inspired by experiments with the 173Mv1 that suggested a means to improve performance at high voltage without the use of trim coils.

In the 173Mv2, the primary circuit consists of the fixed magnetic structure, an inner coil (IC) and an azimuthal outer coil (OC). Both thrusters have an internal trim coil (ITC); the 173Mv2 has an external trim coil (ETC) as well.

The ITC primarily affects the radial magnetic field in the discharge chamber.[6-7] When the coil is energized, the radius of curvature of the

plasma lens (i.e., the axial gradient of the magnetic field, $\nabla_z B_r$) can be changed, depending on the direction of the coil current. By convention, a negative current subtracts from the magnetic field and increases the value of $\nabla_z B_r$.

The ETC is an azimuthal coil located on the outer radius of the thruster body (not shown in Figure 4). The ETC alters the magnetic field downstream of the exit plane and near the cathode. By convention, a negative coil current subtracts from the magnetic field. Reference 9 discusses an approach that uses external coils and poles to affect plume divergence and thrust vectoring in an SPT-100.

The plasma discharge was powered by a matching pair of commercially available power supplies wired in series that provided a 1200 V, 16 A output. The discharge filter consisted of a 100 μF capacitor in parallel with the supply outputs. Other commercially available power supplies were used to power the magnet coils, cathode heater and cathode keeper. The hollow cathode was a 20 A laboratory model fabricated at GRC and positioned above the thruster (see Figure 4).

Xenon (99.999% pure) was supplied through stainless steel feed lines with 20 and 200 sccm mass flow controllers. The controllers were calibrated before, during and after the experiments using a constant-volume method. The estimated uncertainty of the calibrations was ±0.9% for the anode and ±1.0% for the cathode.

Thruster telemetry was acquired using a 22-bit datalogger. The DC accuracy of the unit, as reported by the manufacturer, is 0.004%. However, calibration of each channel using digital multimeters increased the uncertainty to ±0.05% for voltage and ±0.2% for current.

B. Vacuum facility

All experiments were conducted in vacuum facility 12 (VF12) at GRC. VF12 is a cylindrical, stainless steel chamber 3.0 m in diameter by 9.6 meters in length. The facility is cryogenically pumped and backed by a turbomolecular pump for removal of low molecular weight gases that are not pumped by the cryosurfaces. The thruster was mounted near the chamber's centerline on one end of the facility and fired 8.9 m down the length of the tank toward the pumps, which are located along the back half of the chamber. A hot-cathode ionization gauge was mounted 0.4 m below the vertical chamber centerline, 5.2 m downstream from the thruster. Pressure measurements were corrected for xenon using the base pressure on air and a correction factor of 2.87 for xenon. For xenon flow rates of 5, 10 and 15 mg/s, typical pressures were 2.7×10^{-6}, 4.6×10^{-6}, and 6.7×10^{-6} Torr, respectively, after correcting for xenon and the base pressure on air, which was 1.8×10^{-7} Torr. This corresponded to an average xenon pumping rate of 290,000 l/s. At these pressures and flow rates, ingested neutrals from the ambient tank environment have been shown to have a negligible influence on performance measurements.[10]

C. Thrust stand

Thrust was measured using a null-mode, inverted pendulum thrust stand designed at GRC and used previously in VF12.[11] Inclination was controlled by leveling the stand via a stepper motor mechanism to maintain a constant inclinometer output. A water-cooled shroud that encompassed the thrust stand components was maintained at 10° C to minimize thermal drift. Thermal drift was equivalent to no more than 0.5 mN and was quantified through frequent shutdowns (about every 30 minutes), to record the zero offset. Calibrations using a series of known weights were performed every two to four hours before and after several of these firings. Since the slope of the calibration curve was highly repeatable throughout testing, the zero offset recorded after each shutdown was used to obtain the calibration curve valid at the time of shutdown. Linear interpolation over time during each thruster firing yielded the zero offset and, thus, the true calibration curve for each data point as a function of time. Using these methods, the uncertainty in the thrust measurements was estimated to be no more than ±0.5 mN.

The engine was operated for approximately 25 hours before thrust data were collected and the data were collected over hours 25–57 of thruster operation. Upon initial exposure to vacuum, the thruster was operated for three to four hours to allow for outgassing. If the thruster had been off for more than a few minutes, an initial firing of at least 30 minutes was done before data was collected. This ensured that the thruster and thrust stand had equilibrated sufficiently to minimize thermal drift. Repeatability was quantified by returning to certain operating points over the three week testing period and was influenced more by the thruster (e.g., by returning to the same discharge current) than the thrust stand. Using these methods, variations in thrust for a given operating point were 1.0%, on average.

D. Faraday probe

Ion current density measurements were taken using a Faraday probe that has been used

previously at GRC and characterized in other investigations.[12,13] The probe consisted of a 1.94 cm diameter collection electrode enclosed within a guard ring. The guard ring and collector were made from stainless and were biased –15 V below facility ground to repel electrons. The probe face was aligned 98.5 cm downstream of the exit plane, with the axis of rotation located on thruster centerline at the exit plane. An angular coordinate system was defined such that thruster centerline was referenced as zero degrees. When viewed downstream from the exit plane angles became increasingly positive when the probe was swept clockwise. Sweeps were performed from –100° to +100° in 1° increments. At each location, 1000 data points were sampled at 1 kHz and averaged using a 16-bit data acquisition card and a 502 Ohm precision resistor. Data was collected over hours 36–39 and 50–59 of thruster operation.

E. Discharge current probe

A 500 MHz oscilloscope and a 50 MHz current probe were used to monitor discharge current oscillations. The probe was located after the output filter described in section II.A. The oscilloscope sampled the current at 250 kHz. The power spectral density was computed from the discrete Fourier transform of the data with Parzen windowing. Data was collected over hours 36–39 and 50–59 of thruster operation.

III. RESULTS AND DISCUSSION

A. Performance

Performance was evaluated over 300–1000 V at 5 and 10 mg/s and 300–600 V at 15 mg/s. By testing at constant flow rates, current density was held approximately constant as the voltage increased, which was equivalent to increasing the power density. The maximum power at which the thruster could safely be operated was determined to be 10 kW, so no data were generated beyond this power level. (All data are tabulated in Table 1 of the appendix).

The thrust-to-power (T/P) ratio was computed based on the discharge power (V_d*I_d) and the total power, which includes the power dissipated in the coils. Both "anode" and "total" quantities were computed for Isp and efficiency. Anode quantities include only the anode flow and discharge power. Total quantities add the cathode flow and the power required by the coils. The cathode flow was maintained at 10% of the anode flow to ensure there was a sufficient supply of electrons for neutralization and ionization. No attempts were made to optimize the cathode flow, cathode position, or to minimize the power dissipation of the coils. Improvements to the total Isp and efficiency should be possible if the cathode and coils are later optimized.

The general method for taking data was to set the voltage and flow rate and then investigate the effects of each coil on discharge current, plasma oscillations and anode efficiency. It was observed that the effects of the ITC and the ETC on the performance were mostly independent. It was therefore decided to record data first with the ITC energized, then with both the ITC and ETC. This method was used only when both coils were beneficial to efficiency. For example, if the ITC showed no benefit, only ETC data were reported in Table 1 of the appendix.

Once a general range of coil currents yielding near-optimum efficiency was found, data were recorded at several coil currents to ensure that performance was indicative of the optimum. Only data at the optimum coil currents are included in the appendix. Peak performance was generally realized where the discharge current and oscillations were minimized. However, there were cases when the discharge current would increase with efficiency when the trim coils were energized. Because of the breadth of this performance mapping, no systematic attempts were made to quantify the functional relationship of the coils beyond those just described.

The thruster was stable and capable of sustained operation (from tens of minutes to hours) during the period when data at a given operating point was recorded. At voltages greater than 300 V, the thruster became unstable for 10–30 minutes after the voltage was increased. This was attributed to plasma oscillations associated with shifts in the acceleration layer position towards the anode. Internal probe measurements have confirmed the movement of the acceleration layer with voltage.[14] If the voltage was increased rapidly, oscillations would sometimes cause the discharge to extinguish. Movement of the acceleration layer resulted in a gradual lengthening of the discharge chamber erosion band. A "burn-off" period at 600 V or more first confirmed this. This burn-off was qualified by visually observing the erosion layer glowing orange-red at its upstream boundary. Burn-off was observed only above 600 V, but it most likely occurred to a lesser extent at all voltages. The burn-off was quantified by an increase in the discharge current and a decrease in efficiency. The thruster was unstable during burn-off unless the coil currents were increased by a few Amperes. After the burn-off period at each voltage, which lasted 10–30 minutes, the coil currents could be reduced.

Discharge current also decreased after burn-off and the efficiency increased. Additionally, after burn-off the voltage could be decreased and increased back to the burn-off voltage as quickly as the power supply could accommodate the change.

In the following figures, different combinations of coils are shown. The label, "No TC's" refers to operation of the IC and OC only. The other labels follow conventions described earlier. Figures 5–11 are plots of the data from Table 1 of the appendix. Figures 5–8 show how the trim coils affected thruster operation. Specifically, Figure 5 considers the current-voltage characteristics at each flow rate and Figures 6–8 plot the total efficiency versus voltage at 5, 10, and 15 mg/s, respectively. Figures 9–11 show the performance quantities from the coil combinations in Figures 6–8 that maximized efficiency.

The functional relationship of the discharge voltage and current is depicted in Figure 5. The current was found to slowly increase with voltage. In general, the trim coils reduced the current and increased thrust (see Table 1 in the appendix) at a fixed voltage. The increase of current with voltage can be caused by increases in the electron current and/or multiply-charged ions. Probe diagnostics to measure the electron current and ion species fractions as a function of voltage are currently being developed.[14]

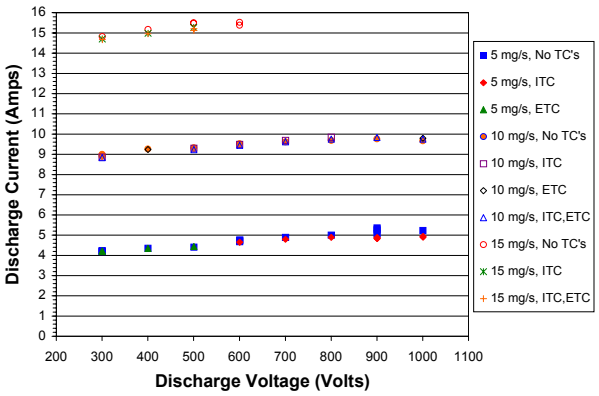

Figure 5 – Current-voltage characteristics at 5, 10, and 15 mg/s.

Figures 6–8 plot total efficiency versus voltage for flow rates of 5, 10, and 15 mg/s, respectively. At a given flow rate and voltage, efficiency was improved or remained unchanged by using the trim coils. When efficiency was unchanged, there were still benefits to overall performance as thrust usually increased. In Figure 6, the efficiency at 5 mg/s shows trends that are very similar to the 173Mv1 data shown in Figure 3. Both thrusters had a maximum efficiency when no trim coils were used (that occurs at 500 V in the 173Mv2 and 600 V in the 173Mv1). Additionally, when the trim coils were used efficiency was shown to increase with voltage for both thrusters. For example, in the 173Mv2 at 300 V, the trim coils improved efficiency by 0.6%, while at 1000 V the efficiency increased by 5.6%. The 173Mv2 showed no improvement with the ITC at 500 V or less; only the ETC was effective. Above 500 V, only the ITC increased efficiency in the 173Mv2. Further, positive ITC currents were found to improve efficiency in the 173Mv2 at 5 mg/s, while negative currents were always beneficial in the 173Mv1.[7] Positive ITC current decreases $\nabla_z B_r$ along the channel. Since $\nabla_z B_r$ is steeper in the 173Mv2 than the 173Mv1, this implies an optimum value of $\nabla_z B_r$ at 5 mg/s, which can be determined by comparing the magnetic fields in both thrusters.

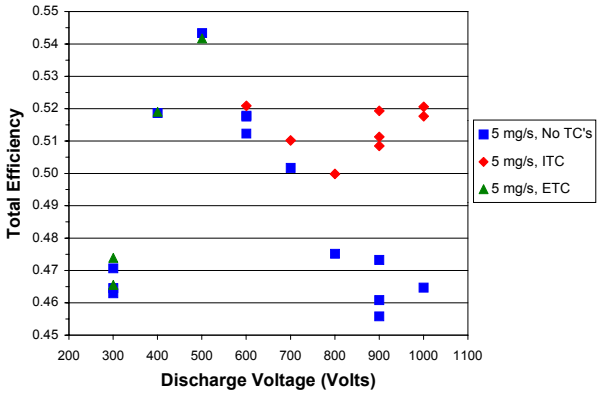

Figure 6 – Total efficiency versus discharge voltage at 5 mg/s.

Figure 7 shows that total efficiency at 10 mg/s increased monotonically with voltage. Total efficiency at 10 mg/s spanned the range of 52.7% at 300 V to 60.8% at 1000 V. Although 1000 V, 10 mg/s operation was near the power limit of 10 kW, the thruster was operated for one hour at this setting. The efficiency at 10 mg/s increased with voltage whether or not the trim coils were used, which indicated improvements to the field topography in the 173Mv2 with respect to the 173Mv1 were near the optimum required for high specific impulse operation.[∀] Unlike the data at 5 mg/s in Figure 6 that shows efficiency improved by as much as 5.6%, using trim coils at 10 mg/s improved efficiency by only 1–2%. Overall, differences between the 5 and 10 mg/s efficiency data imply there is a minimum current density necessary for high efficiency operation in the 173Mv2.

In Figure 8, the efficiency at 15 mg/s shows trends that are similar to Figure 7, albeit at

[∀] This conclusion was supported by data from the 173Mv1 at 10 mg/s (to be published at the 2003 Joint Propulsion Conference) that shows a plateau in the efficiency characteristic at high voltage.

higher efficiencies. Total efficiency was 59.0% at 300 V and increased to a maximum of 63.3% at 600 V. Anode efficiencies exceeded 70% at 500–600 V. As noted earlier, data at 600 V was close to the 10 kW power limit of the thruster. It was difficult to maintain the discharge at 600 V for more than twenty minutes, which did not allow time to experiment with the ITC or ETC. Difficulties sustaining the discharge seemed to be driven more by the combined influence of current and power density—rather than the power density alone—since the thruster was operated for an hour at 1000 V, 10 mg/s.

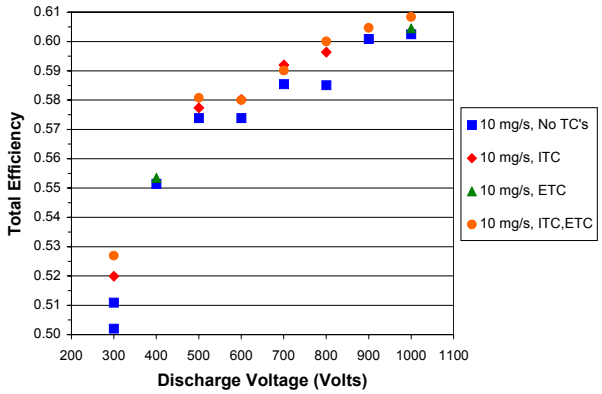

Figure 7 – Total efficiency versus discharge voltage at 10 mg/s.

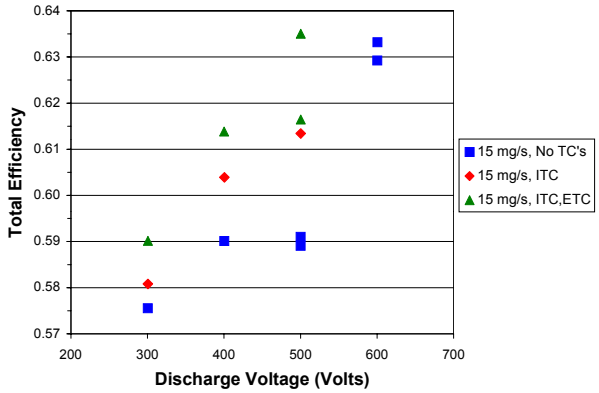

Figure 8 – Total efficiency versus discharge voltage at 15 mg/s.

The total efficiency, total specific impulse and T/P ratio (based on discharge power) for flow rates of 5, 10, and 15 mg/s are shown in Figures 9–11. For clarity, only data from the coil combinations that maximized efficiency at each point are shown. In Figure 9, the trends in total efficiency emphasize the importance of current density in achieving optimal performance. At a fixed voltage, efficiency improved at each higher flow rate because mass utilization is known to increase with current density. Current density also has a role in optimizing efficiency with increasing voltage, as shown by the contrasting efficiency characteristics at 5 and 10 mg/s.

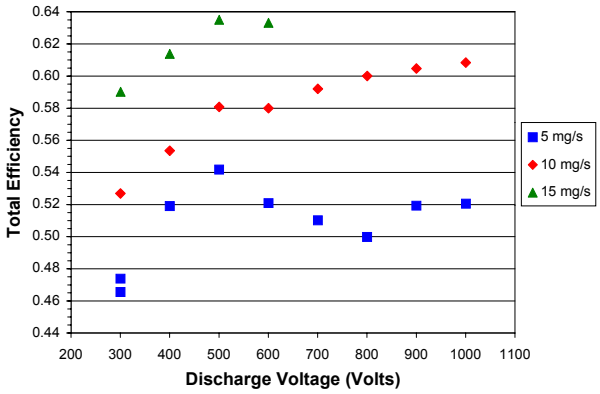

Figure 9 – Optimized total efficiency versus discharge voltage at 5, 10, and 15 mg/s.

Figure 10 shows the total specific impulse at each flow rate. The maximum total specific impulse was 3390 s at 1000 V, 10 mg/s. The specific impulse also increased, like efficiency, with current density at a fixed voltage because of improved mass utilization. However, unlike efficiency, the specific impulse always increased with voltage at a constant mass flow rate. This was because the thrust always increased with voltage, which was expected since thrust and Isp scale as $T \propto Isp \propto V_d^{1/2}$.

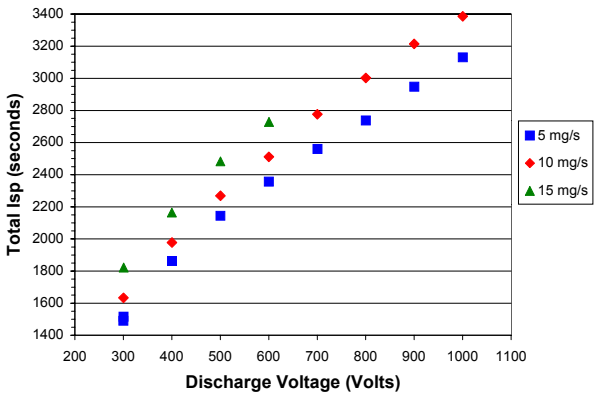

Figure 10 – Optimized total specific impulse versus discharge voltage at 5, 10, and 15 mg/s.

Trends in efficiency and specific impulse are best understood by considering the T/P ratio, shown in Figure 11. The T/P ratio showed a weak dependence with current density at 300–500 V. At 600 V or above, the T/P ratio at 5 mg/s decreased faster than at 10 mg/s, which corresponded to the decrease in efficiency shown in Figure 9. The drop in efficiency can be understood by considering the scaling of the T/P ratio with voltage. At a constant flow rate, efficiency scales as $\eta \propto T^2/P \propto T/P * V_d^{1/2}$. Thus, if the T/P ratio scales with voltage at a power of less than –½, the efficiency will decrease. A power law curve fit to the 5 mg/s data in Figure 11 shows that $T/P \propto V_d^{-0.54}$, while the 10 mg/s data scales as $T/P \propto V_d^{-0.48}$.

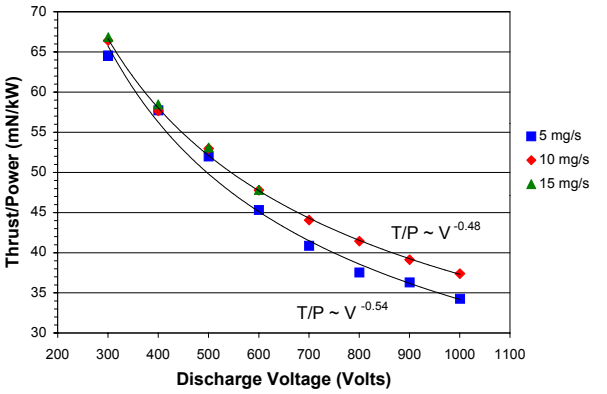

Figure 11 – Optimized thrust-to-power ratio versus discharge voltage at 5, 10, and 15 mg/s. Power law curve fits are shown for 5 and 10 mg/s.

Overall, the performance and operating characteristics of the 173Mv2 highlight the challenges of operating HETs over a large range of current and power densities. Depending on the application, the challenge is maintaining efficient operation without exceeding current and power density limitations. In a constant current application, throttling from 300 to 1000 V requires an increase in the power density by more than a factor of three. This may not be an issue, however, since data at 10 mg/s has shown the 173Mv2 was stable over these power densities. In constant power applications, however, problems may arise if the throttling range is beyond the thermal capabilities of the thruster. This is because at the highest voltage, the thruster should be sized to yield acceptable efficiency. Throttling at constant power to a lower voltage will then increase the current density. Recall that operation of the 173Mv2 at 600 V, 15 mg/s was only sustained for twenty minutes as opposed to 1000 V, 10 mg/s, which was sustained for an hour. Both of these operating points are nearly the same power density, but current density is 50% higher at 15 mg/s than at 10 mg/s. This underscores the importance of current and power density considerations that could limit the throttling range in constant power applications.

B. Ion current density

Plume measurements and plasma oscillation data were collected concurrently after determining optimum coil currents for a given voltage and flow rate. Ion current density measurements were made at 10 mg/s at voltages of 300–1000 V. At all voltages, plume profiles with the IC and OC alone were measured. At 300–600 V, the ITC and the combined influence of the ITC and ETC were documented. At 700–1000 V, only sweeps with the ITC and ETC were performed, with the exception of 1000 V which includes a sweep with the ETC.

Figure 12 shows results from 300–600 V and Figure 13 includes data from 700–1000 V. For clarity, both figures include only the data with the ITC and ETC. Differences in the plume profiles with the other coils are quantified by calculating the plume divergence. Figure 14 shows plume divergence half-angle versus voltage for all combinations of coils that were investigated. Plume divergence was defined as the half-angle from centerline that integrates to 95% of the total current density integrated over ±90°. No attempts were made to account for the effects of the charge exchange plasma due to the finite pumping speed of the facility. Figure 14 shows divergence reached a maximum of 38° at 400 V and a minimum of 28° at 1000 V.

The double peak structure of the ion current density profiles in Figures 12 and 13 was attributed to the annular geometry of the discharge chamber. The current density peaks were more pronounced as the voltage increased, indicating more of the ion current was located near centerline. It is likely that the asymmetry in the profiles was the result of azimuthal non-uniformity of the neutral gas distribution. Because of the favorable performance characteristics, these asymmetries were not believed to significantly affect thruster operation.

Plume divergence angle, shown in Figure 14, is determined by a number of processes, including: radial electric fields in the acceleration zone, the axial location of the acceleration zone, thermal spreading at the ion acoustic velocity, particle scattering in the plume and even plasma oscillations.[15-18] How these processes scale, and which ones dominant, is not completely understood, but divergence should scale as the ratio of radial to axial ion velocity. Thus, a decreasing divergence angle with voltage implies axial velocities are increasing faster than radial velocities. In Figure 14, an increase in divergence was shown between 300–400 V, followed by a continual decrease. The initial increase was attributed to a jump in plasma oscillations (see Figure 18). Excluding the 300 V data, the divergence was found to decrease from 400–1000 V as $\theta \propto V_d^{-0.08}$. Assuming that radial electric fields and thermal expansion dominate the radial expansion, it is easily shown that the electron temperature controlling divergence was scaling as $T_{e,D} \propto V_d^{0.84}$. Numerical simulations (with zero wall losses) by Ahedo are in close agreement, which suggested the electron temperature at the sonic transition in the discharge chamber scales as $T_{e,S} \propto V_d$.[19]

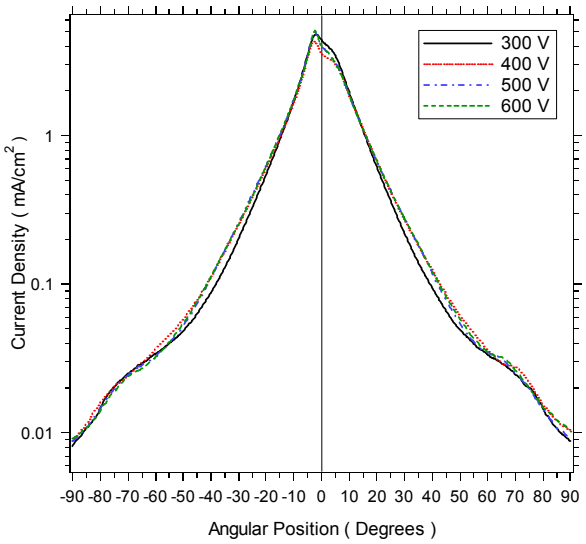

Figure 12 – Ion current density versus angular position at 10 mg/s, 300–600 V with both trim coils (ITC, ETC).

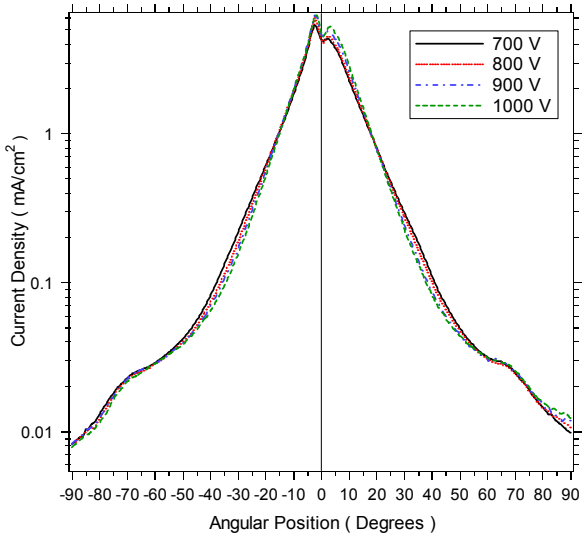

Figure 13 – Ion current density versus angular position at 10 mg/s, 700–1000 V with both trim coils (ITC, ETC).

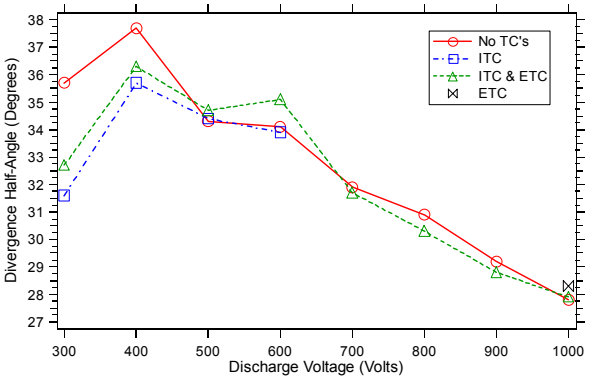

Figure 14 – Divergence half-angle versus discharge voltage at 10 mg/s.

Figure 14 shows that the ETC increased divergence, while the ITC decreased divergence. For example, at 1000 V the ETC increased divergence, but when the ITC was added, a drop was observed. Data at 300–600 V also shows that the divergence decreased with the ITC and then increased when the ETC was added. Further, the cathode potential data in Table 1 of the appendix, which is a measure of the electron coupling with the discharge, shows that the ETC increased the cathode potential (i.e., decreased the magnitude with respect to ground). Taken together, the divergence and cathode potential trends indicate that the ETC improved efficiency by acting primarily on the electrons. Probe measurements of the floating potential have also supported this conclusion.[14]

The effects of the ITC are more complex than the ETC because the ITC alters the magnetic field inside the discharge chamber. Figure 14 shows that the ITC decreased divergence while the data in Table 1 of the appendix shows (with few exceptions) that the cathode potential became more negative, the discharge current decreased and the thrust increased. The changes in cathode potential and discharge current imply the ITC is decreasing the axial mobility of electrons to the anode, while the increase in thrust suggests that the mass utilization is improved when the ITC is used.

C. Plasma Oscillations

Discharge current oscillations at 300–1000 V, 10 mg/s were measured at the same coil combinations as the ion current density. Representative plots of the power spectral density (PSD) at 300 and 1000 V are shown in Figures 15 and 16. In Figure 17, the frequency at which the PSD was greatest is plotted, and Figure 18 plots the standard deviation of the discharge current, expressed as a percentage of the mean discharge current.

In Figures 15–16, the trim coils are shown to affect the PSD at 300 and 1000 V. Figure 15 at 300 V shows how the broadband distribution without trim coils was replaced by a much stronger peak when the trim coils were used. This peak is referred to as the dominant oscillation frequency and is usually associated with the breathing-mode ionization instability.[17] Adding the ETC to the ITC broadened the distribution, but the use of both coil combinations resulted in less broadening than when both were not used. The dependence of the standard deviation (see Figure 18) with the use of trim coils was weak at 300 V, indicating that more of the energy was being concentrated into a narrower band of frequencies.

Figure 16 shows the PSD at 1000 V. In this figure, note that operation with only the ETC, and then the combined influence of the ITC and ETC are shown. The ETC data at 1000 V showed broadening similar to when the ETC was added to

the ITC at 300 V. A primary difference between 300 and 1000 V was the presence of a new oscillatory mode in the 80–90 kHz frequency band. This mode was present at all voltages between 500–1000 V and overall the ETC excited the mode, while the ITC had a dampening influence. Gascon considered the voltage dependence of plasma oscillations experimentally at 300–600 V.[20] This work showed high-frequency modes developing above 300 V. Since these modes were observed at 50–65 kHz in an SPT-100ML, it is not known if they are the same instability. Choueiri has also considered plasma oscillations in the 25–100 kHz range, but his analysis was restricted primarily to the effects of the magnetic field.[17] Future investigations are planned to improve the resolution in the 50–100 kHz frequency band before reaching further conclusions.

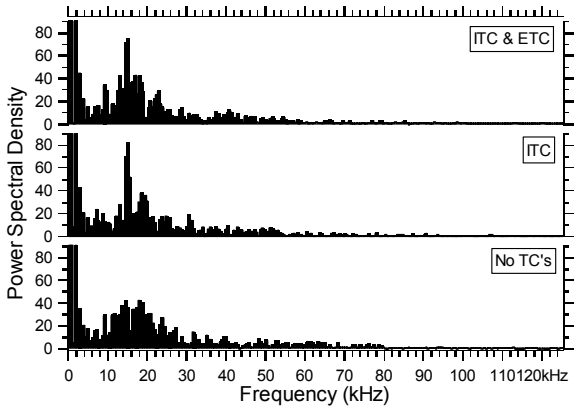

Figure 15 – Discharge current power spectral density versus frequency at 300 V, 10 mg/s.

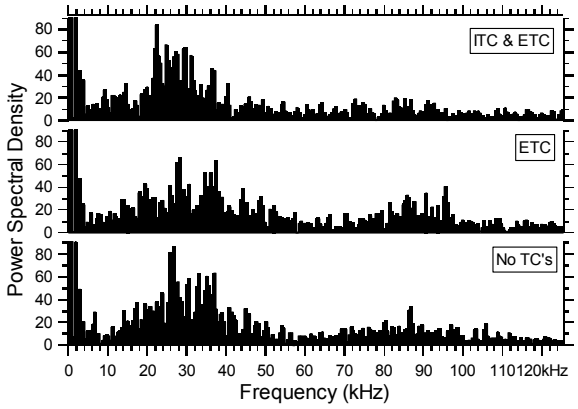

Figure 16 – Discharge current power spectral density versus frequency at 1000 V, 10 mg/s.

As shown in Figure 17, there was a gradual shift to higher frequencies of the dominant oscillation frequency, from 14.5 kHz at 300 V to 22 kHz at 1000 V. The trim coils generally lowered the dominant frequency at each voltage. For example, at 300 V the dominant frequency decreased from 17.5 kHz to 14.5 kHz when the trim coils were used. At 1000 V, the dominant oscillation frequency marginally increased from 26.5 kHz to 28 kHz with the ETC, then dropped to 22 kHz when the ITC was added.

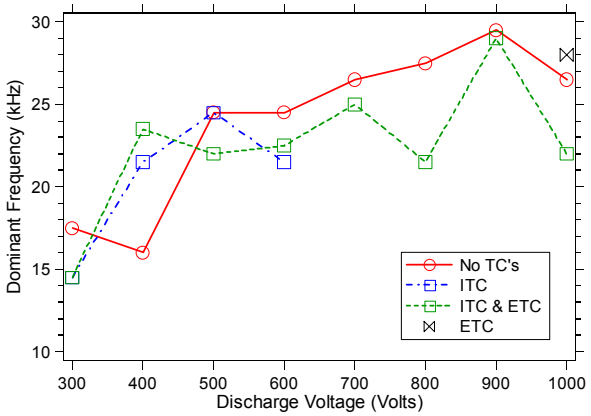

Figure 17 – Dominant frequency from the power spectral density of the discharge current oscillations versus discharge voltage at 10 mg/s.

As shown in Figure 18, there was a large increase in the standard deviation of plasma oscillations between 300 and 400 V, which persisted until 600 V. At 700–1000 V, the standard deviation dropped again to another plateau. In general, the trim coils decreased the magnitude of oscillations at a fixed voltage. The increased oscillations roughly coincided with the range of voltages where efficiency peaked in other HETs (i.e., 500–800 V).[3-5,7] It may be that efficiency begins to drop in other thrusters at a critical voltage due to increased discharge current oscillations. Oscillations can increase the turbulent conductivity of electrons resulting in greater axial electron current. This is thought to be an indication that plasma oscillations are playing a significant role determining efficiency with increasing voltage. Experiments to more firmly establish the connection between the magnetic field, plasma oscillations and electron current are continuing.

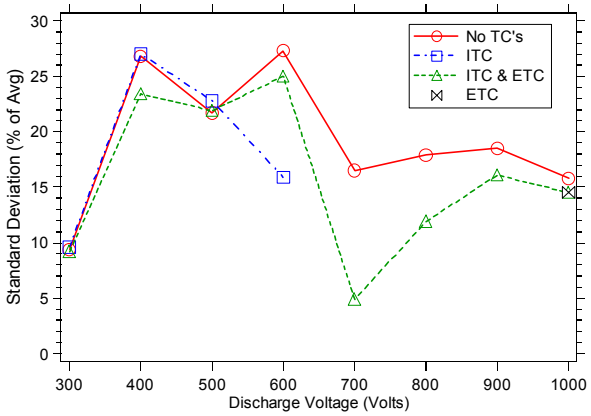

Figure 18 – Standard deviation of the discharge current, as a percentage of the average current, versus discharge voltage at 10 mg/s.

IV. SUMMARY

These experiments have documented the influence of current density and magnetic field topography on the performance, plume divergence and plasma oscillations of high specific impulse Hall thrusters. The key results include:

1. The elimination of a peak in the efficiency-voltage characteristic observed in other xenon Hall thrusters. Operating above a critical current density, and with magnetic fields appropriate for high-voltage, resulted in a monotonic efficiency-voltage characteristic. While enhancing performance overall, trim coils were not required to obtain these results, demonstrating that traditional magnetic circuits can still be used if the fixed field topography is properly instituted.
2. At 1000 V, 10 mg/s, the total specific impulse was 3390 s with a corresponding total efficiency of 60.8%.
3. Trim coils have been shown to affect favorably both plume divergence and plasma oscillations. This may ultimately prove to be their greatest utility, as controlling divergence and oscillations are critical to extending thruster lifetime.
4. Plume divergence was shown to decrease over the range of 400–1000 V from a maximum of 38° to a minimum of 28°. An increase in divergence from 300 to 400 V was attributed to plasma oscillations.
5. The dominant oscillation frequency steadily increased with voltage, from 14.5 kHz at 300 V to 22 kHz at 1000 V.
6. It was shown that the trim coils influenced the magnitude and frequency content of plasma oscillations. An external trim coil broadened the power spectral density while an internal trim coil localized the energy to a narrower band of frequencies.
7. The emergence of additional oscillatory modes in the 80–90 kHz band when the discharge voltage exceeded 500 V has been reported. Trim coils have also been shown to have an effect on this frequency band.

ACKNOWLEDGEMENTS

The authors would like to thank Chris Griffiths for substantially improving the 173Mv2 mechanical design from that of its predecessor, and Kevin Blake for thruster assembly and installation support.

REFERENCES

1. Jankovsky, R. S, Jacobson, D. T., Sarmiento, C. J., Pinero, L. R., Manzella, D. H., Hofer, R. R., Peterson, P. Y., "NASA's Hall Thruster Program 2002," AIAA-2002-3675, 38th Joint Propulsion Conference, Indianapolis, IN, July 7-10, 2002.
2. Manzella, D. H., Jankovsky, R. S., Hofer, R. R., "Laboratory Model 50 kW Hall Thruster," AIAA-2002-3676, 38th Joint Propulsion Conference, Indianapolis, IN, July 7-10, 2002
3. Jacobson, D. T., Jankovsky, R. S., Rawlin, V. K., Manzella, D. H., "High Voltage TAL Performance," AIAA-2001-3777, 37th Joint Propulsion Conference, Salt Lake City, UT, July 8-11, 2001.
4. Manzella, D. H., Jacobson, D. T., Jankovsky, R. S., "High Voltage SPT Performance," AIAA-2001-3774, 37th Joint Propulsion Conference, Salt Lake City, UT, July 8-11, 2001.
5. Pote, B., Tedrake, R., "Performance of a High Specific Impulse Hall Thruster," IEPC-01-035, 27th International Electric Propulsion Conference, Pasadena, CA, Oct 14-19, 2001.
6. Hofer, R. R., Peterson, P. Y., Gallimore, A. D., "A High Specific Impulse Two-Stage Hall Thruster with Plasma Lens Focusing," IEPC-01-036, 27th International Electric Propulsion Conference, Pasadena, CA, Oct 14-19, 2001.
7. Hofer, R. R., Gallimore, A. D., "The Role of Magnetic Field Topography in Improving the Performance of High-Voltage Hall Thrusters," AIAA-2002-4111, 38th Joint Propulsion Conference, Indianapolis, IN, July 7-10, 2002.
8. Morozov, A. I., "Focusing of Cold Quasineutral Beams in Electromagnetic Fields," Soviet Physics – Doklady, Vol. 10, No. 8, Feb. 1966.
9. Day, M., Kim, V., Kozlov, V., Lazurenko, A., Popov, G., Skrylnikov, A., "Investigation of the Possibility to Reduce SPT Plume Divergence by Optimization of the Magnetic Field Topology in the Accelerating Channel," IEPC-97-154, 25th International Electric Propulsion Conference, Cleveland, OH, August 24-28, 1997.
10. Hofer, R. R., Peterson, P. Y., Gallimore, A. D., "Characterizing Vacuum Facility Backpressure Effects on the Performance of a Hall Thruster," IEPC-01-045, 27th International Electric Propulsion Conference, Pasadena, CA, Oct 14-19, 2001.
11. Mason, L. S., Jankovsky, R. S., Manzella, D. H., "1000 Hours of Testing on a 10 Kilowatt Hall Effect Thruster," AIAA-2001-3773, 37th

Joint Propulsion Conference, Salt Lake City, UT, July 8-11, 2001.
12. Manzella, D. H., Sankovic, J. M., "Hall Thruster Ion Beam Characterization," AIAA-95-2927, 31st Joint Propulsion Conference, San Diego, CA, July 10-12, 1995.
13. Walker, M. L., Hofer, R. R., Gallimore, A. D., "The Effects of Nude Faraday Probe Design and Vacuum Facility Backpressure on the Measured Ion Current Density Profile of Hall Thruster Plumes," AIAA-2002-4253, 38th Joint Propulsion Conference, Indianapolis, IN, July 7-10, 2002.
14. Hofer, R. R., Gallimore, A. D., "Recent Results from Internal and Very-Near-Field Plasma Diagnostics of a High Specific Impulse Hall Thruster," IEPC-03-037, 28th International Electric Propulsion Conference, Toulouse, France, March 17-21, 2003.
15. Kim, V., "Main Physical Features and Processes Determining the Performance of Stationary Plasma Thrusters," Journal of Propulsion and Power, Vol. 14, No. 5, Sept-Oct, 1998, pp. 736-743.
16. Martinez-Sanchez, M., Personal Communication, December 2002.
17. Choueiri, E. Y., "Plasma Oscillations in Hall Thrusters," Physics of Plasmas, Vol. 8, No. 4, April 2001.
18. Ashkenazy, J., Raitses, Y., Appelbaum, G., "Parametric Studies of the Hall Current Plasma Thruster," Physics of Plasmas, Vol. 5, No. 5, May 1998.
19. Ahedo, E., Gallardo, J. M., Martinez-Sanchez, M., "Model of the Plasma Discharge in a Hall Thruster with Heat Conduction," Physics of Plasmas, Vol. 9, No. 9, September 2002.
20. Gascon, N., et al., "Signal Processing and Non-linear Behavior of a Stationary Plasma Thruster: First Results," AIAA-99-2427, 35th Joint Propulsion Conference, Los Angeles, CA, June 20-24, 1999.

APPENDIX

Table 1 – NASA-173Mv2 performance data at 300–100 V, 5–15 mg/s.

Vd (V)	Id (A)	Pd (W)	Anode (mg/s)	Cathode (mg/s)	IC (A)	OC (A)	ITC (A)	ETC (A)	Pmag (W)	Ptotal (W)	Thrust (mN)	Thrust/Pd (mN/kW)	Thrust / Ptotal (mN/kW)	Anode Isp (s)	Anode Efficiency	Total Isp (s)	Total Efficiency	Vcg (V)
300.2	4.23	1270	4.99	0.50	1.50	1.20	0.00	0.00	11.3	1281	80.7	63.6	63.0	1650	0.514	1500	0.463	-11.9
300.1	4.19	1257	5.05	0.51	1.50	1.20	0.00	0.00	9.7	1267	80.9	64.3	63.8	1630	0.515	1480	0.465	-12.2
300.2	4.21	1264	5.00	0.50	1.50	1.20	0.00	0.00	9.7	1274	81.2	64.2	63.8	1660	0.522	1510	0.471	-12.0
300.1	4.20	1260	5.05	0.51	1.50	1.20	0.00	-3.00	16.5	1277	81.3	64.5	63.7	1640	0.519	1490	0.466	-11.3
300.2	4.22	1267	5.00	0.50	1.50	1.20	0.00	-3.00	16.7	1284	81.8	64.6	63.7	1670	0.528	1520	0.474	-11.2
400.2	4.35	1741	5.00	0.50	1.70	1.60	0.00	0.00	15.4	1756	100.1	57.5	57.0	2040	0.576	1860	0.519	-13.0
400.2	4.35	1741	5.00	0.50	1.70	1.60	0.00	-4.00	28.2	1769	100.5	57.7	56.8	2050	0.580	1860	0.519	-11.8
500.3	4.41	2206	4.99	0.50	1.56	1.46	0.00	0.00	14.2	2221	115.1	52.2	51.8	2350	0.602	2140	0.543	-12.9
500.3	4.44	2221	4.99	0.50	1.56	1.46	0.00	-3.00	21.4	2243	115.5	52.0	51.5	2360	0.602	2150	0.542	-11.7
600.4	4.73	2840	5.00	0.50	1.85	1.55	0.00	0.00	17.8	2858	126.9	44.7	44.4	2590	0.567	2350	0.512	-12.2
600.5	4.76	2858	5.00	0.50	1.85	1.55	0.00	0.00	17.8	2876	128.0	44.8	44.5	2610	0.573	2370	0.518	-11.1
600.3	4.68	2809	4.95	0.52	1.83	1.55	0.00	0.00	16.7	2826	126.5	45.0	44.8	2610	0.575	2360	0.518	-11.5
600.3	4.65	2791	4.95	0.52	1.83	1.55	0.27	0.00	16.8	2808	126.5	45.3	45.0	2610	0.579	2360	0.521	-11.7
700.3	4.89	3424	4.95	0.52	2.00	1.70	0.00	0.00	20.3	3445	137.5	40.2	39.9	2830	0.558	2560	0.502	-11.1
700.4	4.80	3362	4.95	0.52	2.00	1.70	0.20	0.00	20.5	3382	137.4	40.9	40.6	2830	0.567	2560	0.510	-11.5
800.2	5.00	4001	4.95	0.52	2.67	1.99	0.00	0.00	32.6	4034	144.8	36.2	35.9	2980	0.529	2700	0.475	-10.7
800.2	4.89	3913	4.95	0.52	2.68	1.99	0.52	0.00	33.6	3947	146.9	37.5	37.2	3030	0.557	2740	0.500	-11.4
900.2	5.36	4825	4.95	0.52	2.88	2.32	0.00	0.00	42.9	4868	155.8	32.3	32.0	3210	0.508	2900	0.456	-9.4
900.2	5.26	4735	4.95	0.52	2.77	2.51	0.00	0.00	48.7	4784	155.3	32.8	32.5	3200	0.514	2890	0.461	-8.9
900.3	5.06	4556	4.95	0.52	2.79	2.17	0.00	0.00	42.9	4598	154.3	33.9	33.6	3180	0.528	2880	0.473	-10.8
900.2	4.88	4393	4.95	0.52	2.88	2.32	0.46	0.00	43.6	4437	157.1	35.8	35.4	3240	0.567	2930	0.508	-12.2
900.2	4.84	4357	4.95	0.52	2.88	2.31	0.56	0.00	44.3	4401	156.9	36.0	35.6	3230	0.571	2920	0.511	-12.3
900.2	4.84	4357	4.95	0.52	2.77	2.51	0.56	0.00	48.1	4405	158.2	36.3	35.9	3260	0.580	2950	0.519	-12.5
1000.3	5.23	5232	4.95	0.52	2.99	2.41	0.00	0.00	52.5	5284	163.9	31.3	31.0	3380	0.519	3050	0.465	-9.7
1000.4	4.94	4942	4.95	0.52	2.99	2.41	0.54	0.00	53.7	4996	168.2	34.0	33.7	3460	0.578	3140	0.518	-12.3
1000.4	4.90	4902	4.95	0.52	2.92	2.42	0.57	0.00	53.9	4956	168.0	34.3	33.9	3460	0.582	3130	0.521	-12.6
300.1	8.99	2698	10.00	1.00	1.75	1.49	0.00	0.00	14.3	2712	174.6	64.7	64.4	1780	0.565	1620	0.511	-12.4
300.2	8.90	2672	9.98	1.00	1.75	1.50	0.00	0.00	14.4	2686	172.1	64.4	64.1	1760	0.555	1600	0.502	-12.7
300.2	8.86	2660	10.00	1.00	1.75	1.49	-0.54	0.00	14.6	2674	174.9	65.8	65.4	1780	0.575	1620	0.520	-12.7
300.2	8.84	2654	10.00	1.00	1.75	1.50	-0.54	-4.00	27.4	2681	176.3	66.4	65.8	1800	0.586	1630	0.527	-12.1
400.2	9.26	3706	9.99	1.00	2.50	2.26	0.00	0.00	34.0	3740	212.9	57.4	56.9	2170	0.612	1980	0.551	-13.3
400.2	9.24	3698	9.99	1.00	2.52	2.26	0.00	-1.97	38.2	3736	213.2	57.7	57.1	2180	0.615	1980	0.554	-13.2
500.3	9.32	4663	9.99	1.00	3.00	2.20	0.00	0.00	45.7	4709	243.7	52.3	51.8	2490	0.637	2260	0.574	-13.9
500.3	9.30	4653	9.99	1.00	3.00	2.20	-0.35	0.00	46.3	4699	244.2	52.5	52.0	2490	0.641	2270	0.577	-14.1
500.3	9.23	4618	9.99	1.00	3.00	2.20	-0.35	-5.00	69.0	4687	244.6	53.0	52.2	2500	0.648	2270	0.581	-14.3
600.3	9.52	5715	9.99	1.00	3.26	2.49	0.00	0.00	60.1	5775	269.9	47.2	46.7	2750	0.638	2500	0.574	-13.4
600.3	9.49	5697	9.99	1.00	3.24	2.49	-0.26	0.00	61.6	5758	271.0	47.6	47.1	2770	0.645	2510	0.580	-13.8
600.3	9.44	5667	9.99	1.00	3.24	2.49	-0.26	-5.00	85.4	5752	270.8	47.8	47.1	2760	0.648	2510	0.580	-14.0
700.3	9.61	6730	9.96	1.02	3.41	3.06	0.00	0.00	89.6	6819	296.1	44.0	43.4	3030	0.654	2750	0.585	-13.5
700.3	9.69	6786	9.96	1.02	3.41	3.06	-0.20	0.00	90.7	6877	299.0	44.1	43.5	3060	0.661	2780	0.592	-14.1
700.3	9.62	6737	9.96	1.02	3.41	3.06	-0.20	-5.00	116.2	6853	298.0	44.2	43.5	3050	0.662	2770	0.590	-13.4
800.3	9.68	7747	9.96	1.02	3.82	3.30	0.00	0.00	113.6	7861	317.8	41.0	40.4	3250	0.654	2950	0.585	-13.5
800.3	9.84	7875	9.96	1.02	3.81	3.29	-0.21	0.00	116.3	7991	323.5	41.1	40.5	3310	0.667	3000	0.596	-14.3
800.3	9.75	7803	9.96	1.02	3.81	3.29	-0.21	-4.01	134.6	7937	323.4	41.4	40.7	3310	0.673	3000	0.600	-13.5
900.1	9.76	8785	9.96	1.02	3.85	3.61	0.00	0.00	142.0	8927	343.2	39.1	38.4	3510	0.673	3190	0.601	-14.4
900.1	9.83	8848	9.96	1.02	3.85	3.61	-0.04	-5.90	178.4	9026	346.2	39.1	38.4	3540	0.680	3210	0.605	-13.5
1000.2	9.67	9672	9.96	1.02	4.37	3.81	0.00	0.00	184.1	9856	361.1	37.3	36.6	3700	0.677	3350	0.602	-13.9
1000.2	9.79	9792	9.96	1.02	4.36	3.81	0.00	-5.01	178.4	9970	363.8	37.2	36.5	3720	0.679	3380	0.604	-13.7
1000.2	9.75	9752	9.96	1.02	4.36	3.81	-0.16	-5.00	203.5	9955	364.7	37.4	36.6	3730	0.685	3390	0.608	-13.5
300.4	14.82	4452	14.99	1.50	2.15	1.75	0.00	0.00	24.4	4476	291.5	65.5	65.1	1980	0.637	1800	0.576	-8.9
300.5	14.70	4417	14.99	1.50	2.15	1.74	-0.22	0.00	24.6	4442	291.7	66.0	65.7	1980	0.643	1800	0.581	-9.1
300.6	14.67	4410	14.99	1.50	2.15	1.74	-0.22	-6.00	55.3	4465	294.8	66.9	66.0	2010	0.657	1820	0.590	-8.6
400.4	15.17	6074	14.99	1.50	2.51	2.01	0.00	0.00	34.6	6109	344.8	56.8	56.4	2350	0.653	2130	0.590	-9.3
400.5	14.98	5999	14.99	1.50	2.50	2.00	-0.82	0.00	35.4	6035	346.7	57.8	57.4	2360	0.668	2140	0.604	-9.4
400.1	14.96	5985	14.99	1.50	2.50	2.00	-0.82	-6.00	68.9	6054	350.1	58.5	57.8	2380	0.683	2160	0.614	-8.9
500.1	15.47	7737	15.00	1.50	3.24	2.98	0.00	0.00	75.7	7812	389.7	50.4	49.9	2650	0.654	2410	0.589	-10.9
500.1	15.50	7752	15.00	1.50	3.24	2.99	0.00	0.00	74.8	7826	390.7	50.4	49.9	2660	0.656	2410	0.591	-10.9
500.2	15.27	7638	14.99	1.50	3.24	2.98	-1.24	0.00	78.0	7716	395.1	51.7	51.2	2690	0.682	2440	0.613	-10.9
500.3	15.12	7565	14.99	1.50	3.24	2.98	-1.24	-7.94	139.9	7704	401.7	53.1	52.1	2730	0.712	2480	0.635	-9.5
500.4	15.21	7611	15.00	1.50	3.25	2.99	-1.25	-8.00	171.9	7783	397.9	52.3	51.1	2700	0.693	2460	0.616	-9.3
600.4	15.38	9234	15.00	1.50	3.76	3.25	0.00	0.00	98.4	9333	441.6	47.8	47.3	3000	0.704	2730	0.633	-12.3
600.2	15.52	9315	15.01	1.50	3.75	3.25	0.00	0.00	104.4	9419	442.4	47.5	47.0	3000	0.700	2730	0.629	-11.9